ACS APPLIED MATERIALS & INTERFACES

Research Article

www.acsami.org

Composite WO_3/TiO_2 Nanostructures for High Electrochromic Activity

Karla R. Reyes-Gil,*[,†] Zachary D. Stephens,[‡] Vitalie Stavila,[†] and David B. Robinson[†]

[†]Sandia National Laboratories, P.O. Box 969, Livermore, California 94551, United States

[‡]Sandia National Laboratories, P.O. Box 5800, Albuquerque, New Mexico 87185, United States

Supporting Information

ABSTRACT: A composite material consisting of TiO_2 nanotubes (NT) with WO_3 electrodeposited on its surface has been fabricated, detached from its Ti substrate, and attached to a fluorine-doped tin oxide (FTO) film on glass for application to electrochromic (EC) reactions. Several adhesion layers were tested, finding that a paste of TiO_2 made from commercially available TiO_2 nanoparticles creates an interface for the TiO_2 NT film to attach to the FTO glass, which is conductive and does not cause solution-phase ions in an electrolyte to bind irreversibly with the material. The effect of NT length and WO_3 concentration on the EC performance were studied. The composite WO_3/TiO_2 nanostructures showed higher ion storage capacity, better stability, enhanced EC contrast, and longer memory time compared with the pure WO_3 and TiO_2 materials.

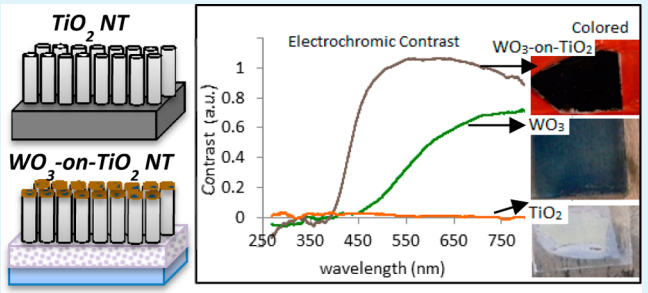

KEYWORDS: *electrochromism, reflectance devices, TiO_2 nanotubes, WO_3 nanostructures, Ti anodization, WO_3 electrodeposition, composites*

1. INTRODUCTION

Electrochromic (EC) materials respond to an applied bias by reversibly changing their spectral absorption properties via a redox reaction. EC materials are of particular interest for their use in smart windows and displays.[1] Smart windows equipped with EC materials give the user the ability to optimize the building's energy use by controlling the amount of light and heat that passes through the window. The largest factor in a building's energy loss to its environment is through its windows; consequently, EC smart windows can decrease the energy used to heat and cool a building by 25%, they can reduce lighting energy requirements by 50%, and they can reduce peak power by 30−40%.[1] EC technology also finds uses in outdoor applications, such as reflectance devices and indoor applications, such as displays, and for privacy purposes in offices and bathrooms. The dynamic layers of the EC windows are mainly manufactured by sputtering, which provides a high degree of control and creates uniform results. However, commercial smart windows (or dynamic windows) still cost up to \$1000 per m^2 of glass. More efficient and cheaper materials are needed to make the electrochromic materials a more attractive commercial option for multiple applications.

Wide-bandgap metal oxides, such as WO_3, Nb_2O_5, and TiO_2, are good candidates for EC devices because their well-defined lattice structures allow easy field-aided ion intercalation, which is needed to accommodate the change in oxidation state in the EC material. In addition, they can be manufactured using low-cost processes such as electrodeposition. Of the transition metal oxides, WO_3 shows the best EC activity, i.e., it has the highest optical contrast, the lowest onset potential, and has sufficient cycling durability.[2−4] WO_3 is pale yellow, and turns dark blue when partially reduced to WO_2. Yu et al. reports a method of electrodepositing thin films of WO_3 onto ITO glass and Ni sheets with good optical contrast, smooth morphology, and good durability after 10,000 cycles.[5] De Tacconi et al. used pulsed cathodic electrodeposition to create composite WO_3/TiO_2 films on conductive glass with small amounts of TiO_2 (W/Ti = 98:2 atom % and W/Ti = 96:4 atom %). They found that composite WO_3/TiO_2 has superior coloration/decoloration dynamics and the blue shift is more pronounced than that of pure WO_3 or TiO_2.[6]

Nanostructures have been investigated in order to enhance the EC contrast and switching speed.[7] The ion intercalation that allows for a change in oxidation state is limited to a very thin surface layer of the electrochromic material. Also, switching speed is controlled by ion transport into a film. Therefore, materials with high surface area could enhance the EC contrast and switching speed.[8] Porous WO_3 can be fabricated that has superior EC properties over compact WO_3.[8,9] Another interesting morphology with high surface area is one-dimensional nanostructures, such as nanotubes and nanorods.[10] However, long nanotubular WO_3 cannot be fabricated easily,[9−11] and therefore the morphological advantages of NT are not retained with WO_3. A strategy explored by

Received: July 31, 2014
Accepted: January 6, 2015
Published: January 6, 2015

DOI: 10.1021/am5050696
ACS Appl. Mater. Interfaces 2015, 7, 2202−2213

Benoit et al. dip coats TiO_2 NT with a solution of WCl_6 to get, after annealing, an inhomogeneous coat of monoclinic WO_3 on the surface of the NT array. The authors concluded that the TiO_2 NT with WO_3 on the surface had increased current densities, more distinct onset potentials, higher contrast, and higher ion intercalation capacity compared to pure TiO_2 NTs.[11] Lai et al. sputter deposited W onto a TiO_2 NT array without breaking the well-oriented, vertically aligned nanotubes, but it was not tested for electrochromic applications.[12] Nah et al. showed that composite TiO_2–WO_3 NTs can be fabricated by anodization of a TiW alloy. Their material, tested in situ on the TiW alloy substrate, has enhanced ion storage capacity and reflectance difference compared with the pure materials.[13] Recently, Cai et al. reported the preparation of TiO_2@WO_3 core/shell nanorod arrays with enhanced electrochromic properties.[14]

This work shows a low-cost synthetic approach to prepare electrochromic films with organized nanostructures that enhance the ion capacity, EC contrast and stability. Previously, we reported the fabrication of composite WO_3/TiO_2 photoanodes using TiO_2 nanotubes as template for WO_3 electrodeposition.[15] Here, we report the fabrication, detachment, and transfer to fluorine-doped tin oxide-coated (FTO) glass of a material with high EC activity made of a layer of TiO_2 NT with WO_3 electrodeposited on the surface. These materials maintain the morphological advantages of TiO_2 NT while exploiting the superior EC activity of WO_3. WO_3/TiO_2 materials show anodic peak current values up to 10 mA/cm^2 at 40 mV/s scan rate, electrochromic contrast of over 95% in the visible range, and excellent cycle stability, demonstrating a significant improvement compared to prior materials. The films are transferred to FTO glass prior to all of the applied EC characterization techniques. This approach has a large commercial potential for the EC smart-glass industry because it produces efficient materials with low manufacturing cost. The method described here should allow the EC films to be incorporated to diverse substrates including existing windows, which could reduce installation costs.

2. MATERIALS AND PROCEDURES

2.1. Preparation of Composite WO_3/TiO_2 nanostructures. *2.1.1. Preparation, Detachment, and Transfer of TiO_2 NTs.* TiO_2 NTs were obtained by Ti foil anodization, as described in our previously published work.[15] Briefly, Ti foil (0.25 mm thick and 99.7% trace metal basis, Aldrich) was cleaned with acetone, deionized water, and methanol and then dried under a stream of N_2 gas. Ti foil was cut in pieces of 2 by 4 cm^2, and the back of the foil was covered with insulating tape. The Ti foil was used as the anode and Pt gauze (100 mesh, 425 mg, 25 × 25 mm^2, Aldrich) as the cathode. A Teflon beaker was used as an electrochemical cell. All the solutions were prepared with analytical graded reagents from Aldrich. The electrolyte solution used was NH_4F (0.3 wt %) in ethylene glycol (EG)/water (ratio of 95:5). The reaction was driven by a dc power supply. All the experiments were carried out at room temperature. The TiO_2 NTs used for the following reactions were prepared via a two-step process. In the first step (pretreatment), a Ti foil was anodized at 50 V overnight (approximately 15 h). Then the nanotube layer was removed ultrasonically in deionized water, and the remaining foil was dried under a stream of N_2 gas. In the second step, the pretreated foil was anodized again with fresh EG/NH_4F/H_2O solution at 50 V. The anodization time was changed to grow NTs of varying lengths to investigate the effect of these different lengths on the material's EC properties. The TiO_2 nanotubes were annealed in air at 500 °C for 2 h to convert the material from an amorphous phase to crystalline anatase.

The membrane was detached from the foil by anodizing it for 0.5 h in the same solution at 50 V to create an amorphous layer of TiO_2, and then the sample was exposed to 0.05 wt % HF to selectively dissolve the amorphous layer, leaving a crystalline TiO_2 NT film. The membrane was submerged in NaOH (0.1 M) to neutralize the pH, and it was cleaned with DI water. The TiO_2 NT membrane was subsequently attached to a conductive fluorine-doped tin oxide film (FTO) on glass using one of a variety of adhesion layers (Hartford Glass Co. Inc., TEC15 (sheet resistance = 15 Ω/square, film thickness = 4000 Angstron and glass thickness = 2.3 mm). The following solutions or pastes were investigated to find a conductive and transparent interface to attach TiO_2 NT films onto FTO glass: (1) TiO_2 P25 paste: 5 g TiO_2 nanopowder (Degussa P25) were mixed with 0.5 mL acetic acid and 8 mL DI water, in a ceramic mortar using a pestle for 15 min. The acetic acid causes strong bonds with the conductive glass.[16] During this procedure, it is important to ensure the mixing and grinding times are enough to avoid producing a nonhomogeneous paste.[16] (2) 0.1 M Ti(i-OPr)$_4$ where i-OPr = 2-propoxide in 2-propanol, (3) neat Ti(OBu)$_4$ where OBu = 1-butoxide, (4) TiO_2 P25 paste with different amounts of Ti(OBu)$_4$, and (5) TiO_2 paste or Ti(i-OPr)$_4$ with different amount of polyethylene glycol 300 (PEG). A layer of paste or liquid was coated onto the FTO glass by tape casting, and then the membrane was transferred onto the glass using the paste/liquid as an interface. The TiO_2 NT-FTO glass samples were successively annealed at 150 °C for 30 min then 450 °C for 1 h to evaporate any solvents and create an anatase TiO_2 layer within the membrane/glass interface.[17] For some samples, a steel sheet was put on top of the membrane to apply pressure during the annealing process.

2.1.2. WO_3 Electrodeposition. WO_3 was electrodeposited in situ while the TiO_2 NT membrane was attached to the FTO glass. The film electrodeposition method is based on the cathodic reduction of a peroxo precursor, which is obtained by mixing a tungsten precursor with hydrogen peroxide. The deposition solution was prepared by dissolving Na_2WO_4 salt (Aldrich) in deionized water and adding concentrated hydrogen peroxide (30%) which can bind to the anion and improve its solubility at low pH. In the resulting solution, the Na_2WO_4 concentration was 25 mM and hydrogen peroxide concentration was 30 mM. The pH of the solution was 10.4 ± 0.1. Nitric acid was added subsequently in order to adjust the pH to 1.4. The solution was prepared the day of the deposition experiments. Either insulating tape or Hysol IC epoxy was used to cover everything except the TiO_2 NT area that was to be electroplated with WO_3. A digital photograph was used to calculate the area using ImageJ software. The electrodeposition experiments were performed in a three-electrode Teflon electrochemical cell at room temperature. The reference electrode was Ag/AgCl and the counter electrode was a Pt gauze. A potentiostat (SP-240, Bio-Logic Science Instruments) was used to apply a potential of −0.437 V vs Ag/AgCl (−0.24 V vs NHE) and record the charge density during the deposition experiments. WO_3. For comparison purposes, the same WO_3 electrodeposition procedure and annealing process were followed using TiO_2 NTs on either Ti foil or FTO glass as the substrates. It has been shown that parallel parasitic reactions take place and should correspond to hydrogen evolution, colloidal WO_3 formation, and reduction of free H_2O_2, residual O_2, and polytungstate. Due to all the parasitic reactions and uncertainty of the deposition efficiency and stoichiometry, we decided to report deposited amounts in deposited charge density (mAh) instead of moles. The resulting composite materials were annealed in air at 400 °C for 2 h to aid crystallization.

2.2. Characterization. The samples on the foil and on the FTO glass were analyzed by scanning electron microscopy-energy-dispersive X-ray spectroscopy (SEM-EDS) and X-ray diffraction (XRD). Rietveld refinements were performed using the software package HighScore Plus. Morphological characterization was carried out by JEOL JSM7600F Thermal Field Emission SEM. Top views of the TiO_2 NT were taken before and after WO_3 electrodeposition. For the cross-sectional views, the foil was bent, and the glass was broken by tracing a scratch with a diamond pen and then applying a tensile bending stress to the scratch. Several areas of the film were analyzed using an EDS

DOI: 10.1021/am5050696
ACS Appl. Mater. Interfaces 2015, 7, 2202–2213

(Oxford XMax with 80 mm^2 detector) that was coupled to the SEM. Crystal structures were collected by Empyrean X-ray diffraction spectrometer and data was analyzed by X'Pert High Score Plus software.

2.3. Testing of Electrochromic Properties. For electrochromic measurements, the samples were placed into an electrochemical cell filled with 0.1 M $HClO_4$. Opposite the sample (approximately 3 cm away), a Pt gauze and Ag/AgCl electrode were used as counter and reference electrode, respectively. An SP-240 potentiostat (Bio-Logic Science Instruments) was used to control the parameters and collected the data. Ion storage capacity was determined by cyclic voltammetry. Switching time was qualitatively analyzed by double potential step chronoamperometry (DPSC). For the optical properties, the reflectance spectra of the films were collected using a Shimadzu UV-2101PC spectrometer with a diffuse reflectance adapter with an integrating sphere. $BaSO_4$ was used as a reference material. An initial spectrum was taken for each sample. Then, after the electrochromic switching, the samples were placed in the spectrometer and data were collected at 5 min intervals. The electrochromic contrast was calculated, subtracting the initial and colored reflectance spectra. Memory time was calculated by taking the time elapsed from the colored state to back to the initial state at open circuit.

3. RESULTS AND DISCUSSION

3.1. Preparation of Composite WO_3/ TiO_2 NT. Figure 1 shows the synthetic approach taken to develop the composite materials. Parallel approaches were developed to prepare WO_3/TiO_2 NT on Ti foil and on FTO glass (or other substrates). The following section discusses the details of each step of the synthetic approach.

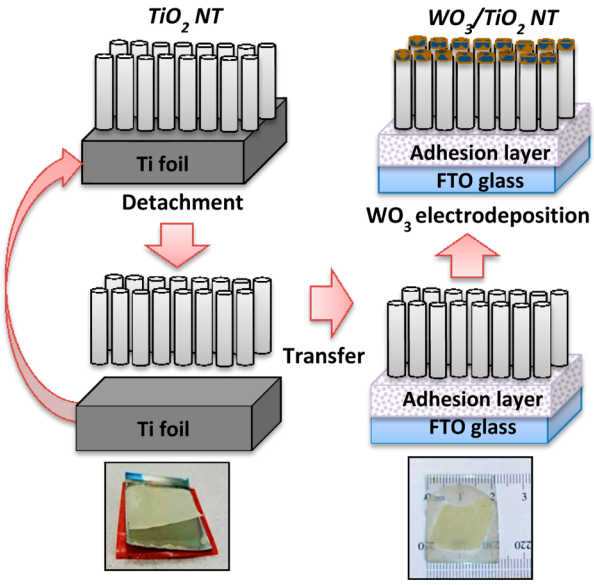

Figure 1. Scheme of the preparation of WO_3/TiO_2 NTs and photographs of the detached and attached membrane to glass.

3.1.1. TiO_2 NT Preparation. SEM images showed that after the first anodization, the TiO_2 nanotubes are in a disordered array due to the corrugated surface of the Ti foil. Below the disordered surface, the TiO_2 NT are very organized, as shown in our previous report.[15] Several pretreatment techniques have been reported to improve ordering, including acid treatment and polishing; however, a better technique for this approach was to peel off the first TiO_2 NT layer and repeat the anodization process as reported in our previous paper.[15] After the nanotube layer was removed ultrasonically, an imprint pattern was left on the foil, which works as template in the further growth of well-aligned nanotubes. After the second anodization, TiO_2 NT are highly uniform and vertically oriented; the opening (mouth) is 100 nm in diameter and the walls are approximately 10 nm thick.

3.1.2. Detach and Transfer of TiO_2 NT and Reuse of Ti Foil. Several methods to detach the TiO_2 NT from the Ti foil have been reported in the literature. One strategy is to use an anhydrous methanol/Br_2 solution to selectively dissolve the Ti substrate and leave the oxide layer.[18] Subsequent etching of the bottom of the membrane by HF will open the NTs but leave a slightly inhomogeneous bottom layer.[19] It is also possible to obtain a free-standing TiO_2 NT membrane by applying a large voltage pulse in situ after the traditional anodization voltage is applied.[20,21] Wang and Liu's version of this procedure allows for control over the diameter of the NT openings on the bottom of the membrane.[21] In this work, the membrane was detached by creating an amorphous thin TiO_2 layer between the Ti foil and the anatase TiO_2 NT by a subsequent anodization after the annealing step. The sample was then exposed to 0.05 wt % HF to selectively dissolve the amorphous layer, leaving a crystalline TiO_2 NT film. Figure 2 shows that the TiO_2 NT preserved the tubular morphology after the detachment process. TiO_2 NT membranes with different thicknesses prepared using different anodization times (5 h, 2 h, 1 h, 50, 30, 20, and 10 min) were successfully detached. The membranes prepared with anodization times less than 30 min were very thin and transparent, but fragile, and consequently difficult to transfer. The dried membrane prepared with longer anodization times were robust and easy to handle with tweezers, but yellowish and opaque (as shown Figure 1). Sizes larger than 1 cm^2 were detached and successfully transferred to the glass. Transferring very thin and transparent free-standing TiO_2 membrane has been a challenge. The

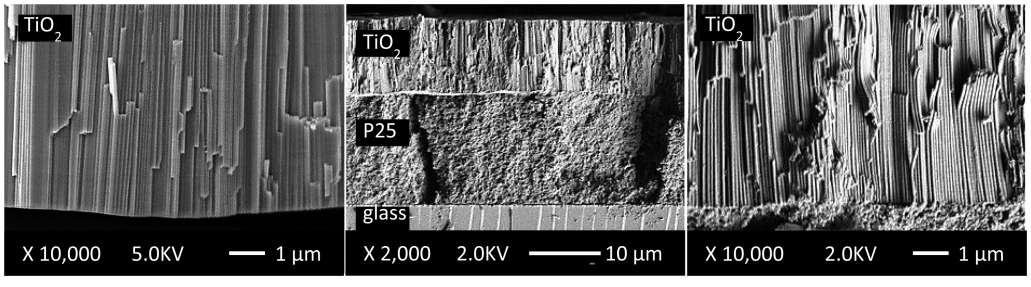

Figure 2. SEM cross sectional images of TiO_2 NT free-standing (left) and attached membrane on P25 layer/FTO glass (center and right). Magnification and scale bar were (left) and (right) 10 000× and 1 μm, and (center) 2000× and 10 μm, respectively. Anodization time was 2 h and the estimated thickness of the TiO_2 NTs was 12.8 μm. SEM images for all the samples in Table 2 are available in SI Figure S2.

DOI: 10.1021/am5050696
ACS Appl. Mater. Interfaces 2015, 7, 2202−2213

membrane that we successfully transferred looks very similar of those reported in the literature.[2,17,19,22]

Several techniques were used to attach the membrane to the glass. When pure $Ti(OBu)_4$ was used as adhesion layer, the membranes detached from the glass after the annealing process. Samples with other adhesion layers did not detach, and were analyzed by cyclic voltammetry (CV) (Table 1). A successful attachment is one that reproducibly shows high conductivity, indicated by high current in the CV, and reversibility, indicated by a ratio of the peak anodic current to the peak cathodic current near 1:1.[23] Perchloric acid is used as the electrolyte because the film is stable under acidic conditions, the perchlorate ion interacts minimally with the film, and H^+ is an effective intercalating ion that is likely to bind to oxygen atoms when the film is in a partially reduced state (all the CV can be seen in the Supporting Information, SI, Figure S1). CV of TiO_2 NT on Ti foil shows a very high conductivity and reversibility. Techniques B–E showed that the interface used to attach the TiO_2 NT to the FTO glass reduced the conductivity and caused the intercalation redox event to be partially irreversible. Techniques A and F showed better reversibility and a higher current density compared to the other techniques. Several more samples were prepared using these two techniques. The results indicate that the reproducibility of the attachment technique for Technique A was poor. However, the results for multiple samples using the Technique F showed that the P25 paste creates an interface for the TiO_2 NT film to attach to the FTO glass that retains the NT conductivity, does not cause irreversible redox reaction, and is reproducible. Due to the success of this attachment technique, further experiments mentioned in this report are attached using this method. However, P25 layer was more dense and opaque than the other adhesion layers based on Ti isopropoxide.

Table 1. Summary of Techniques Used to Attach TiO_2 NT Membranes[a]

label	attachment technique	membrane area (cm^2)	max. anodic current density (mA/cm^2)
A	1 drop 2 month aged 0.1 M $Ti(i\text{-}OPr)_4$	1.5	0.795
B	1 drop fresh 0.1 M $Ti(i\text{-}OPr)_4$	0.5	0.044
C	1 drop fresh 0.1 M $Ti(i\text{-}OPr)_4$ and 2 drops PEG	0.9	0.004
D	1 drop $Ti(OBu)_4$	1.3	0.217
E	TiO_2 paste with 2 drops $Ti(OBu)_4$ and 4 drops PEG	1.4	0.127
F	P25 TiO_2 paste	1.3	0.924

[a]The maximum anodic current density was determined using CV from SI Figure S1.

The Ti substrate was reused for manufacture of several NT membranes sequentially after the membrane is separated, which makes it economical and environmentally favorable. After sequential fabrication with the same Ti substrate, several scanning electron microscope (SEM) micrographs of the membranes and CV experiments were performed. SEM images show little change to the morphology of the membranes. In addition, CV of several TiO_2 NT films prepared from the same Ti substrate showed very similar responses. The results suggest that the reuse of Ti foil does not adversely affect the morphology/performance of the TiO_2 NTs, and it definitely reduces the synthesis costs.

3.1.3. WO_3 Electrodeposition. High quality WO_3 films are most generally obtained by time-consuming and expensive methods such as vacuum evaporation and sputtering. Electrodeposition seems to be very promising approach to create WO_3 films, however the developing of nanostructures has been challenging. The preparation of nanostructured WO_3 films by electrodeposition using TiO_2 NT/Ti foil as a substrate was described in our previously published work.[15] The WO_3/TiO_2 NT on Ti foil was tested for solar photoconversion reactions, showing remarkable improvement in the charge carrier transport and optical properties compared with the parent materials: WO_3 and TiO_2. Here, WO_3 was in situ electrodeposited on TiO_2 NT membrane on FTO glass. TiO_2 NTs have to be annealed before the electrodeposition because amorphous TiO_2 partially dissolves in tungstic acid solution. To the best of our knowledge, this work is the first one to use TiO_2 NT membranes as substrates for in situ WO_3 electrodeposition.

3.2. Characterization of Composite Materials.

3.2.1. Morphology and Elemental Composition. Figure 2 shows the cross sectional images for sample TiO_2 (2 h). The images for all the samples included in Table 2 are available in the SI. To obtain the cross sectional images, the FTO glass was fractured using a diamond pen and mounted at 90°. The length of the TiO_2 nanotubes and the thickness of the P25 layer were calculated using the ImageJ2 software and the scale bar. More than five SEM images were taken at different locations for each sample and the layer thicknesses were measured at different points for each image. The standard deviation and averaged value are reported in Table 2. One representative cross-sectional SEM image for each anodization time (with and without electrodeposited WO_3) can be seen in SI Figure S2. The length of the TiO_2 nanotubes is directly proportional to the anodization time. The thickness of the P25 paste used as the adhesion layer ranges between 14 and 37 μm and depends on the application technique. The nanotubes look very well vertically organized and the P25 layers appear to form a nanoparticle network. The SEM images show good connectivity between the nanotubes and the P25 layer. Some fractured nanotubes and debris can be seen as result of the fracture process.

Figure 3 shows the SEM plain-view images of composite materials on FTO glass. EDS was performed in at least five

Table 2. TiO_2 Nanotube Length and P25 Thickness Calculated from SEM Cross Sectional Images

sample labels	anodization time (h)	WO_3 deposited ($mAh\ cm^2$)	TiO_2 NT length (μm)	P25 thickness (μm)
TiO_2 (1 h)	1	0	5.79 ± 0.03	14.1 ± 0.8
WO_3/TiO_2 (1 h)	1	0.225	6.4 ± 0.7	25 ± 1
TiO_2 (2 h)	2	0	12.8 ± 0.6	17 ± 3
WO_3/TiO_2 (2 h)	2	0.225	11.9 ± 0.3	37 ± 1
TiO_2 (5 h)	5	0	15.8 ± 0.4	16.2 ± 0.6
WO_3/TiO_2 (5 h)	5	0.225	22.2 ± 0.8	24 ± 2

DOI: 10.1021/am5050696
ACS Appl. Mater. Interfaces 2015, 7, 2202–2213

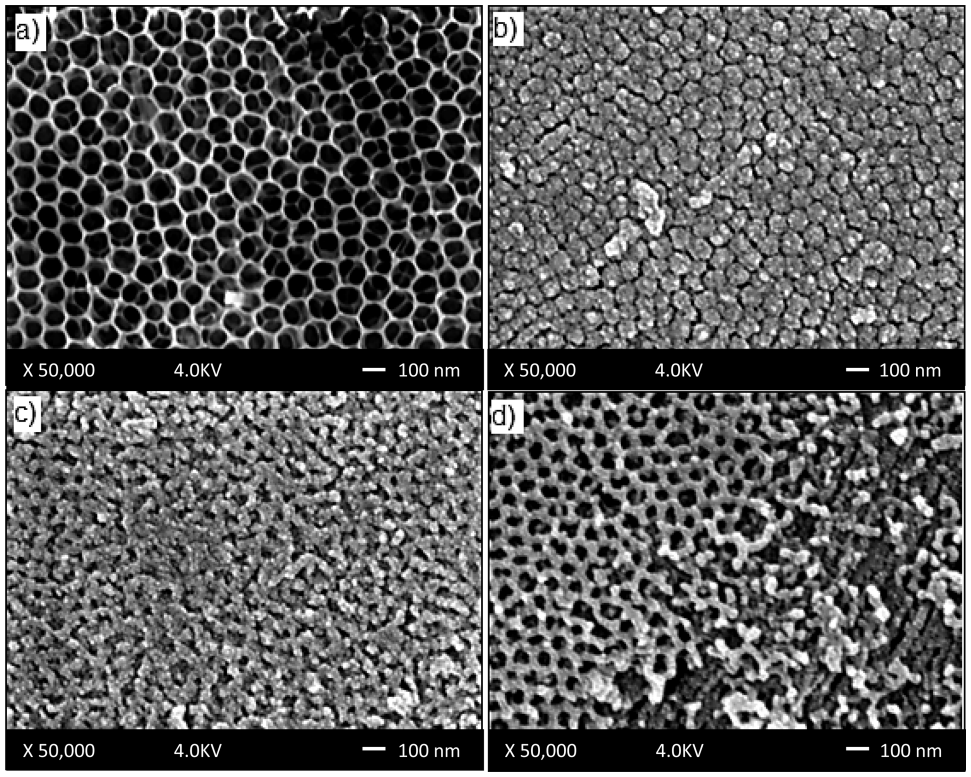

Figure 3. SEM plan-view images of (a) TiO_2 NT and (b–d) WO_3/TiO_2 NT membranes on FTO glass. The anodization time for the TiO_2 NT substrate was (b) 1 h, (c) 2h, and (d) 5h, and (b–d) the WO_3 deposited charge density was 0.225 mA h cm^{-2}. The magnification is 50 000× and the scale bar is 100 nm.

Table 3. Average Atomic Percentages (At. %) of the Main Elements Found in the EDS Spectra

sample labels	Ti anodization time (h)	WO_3 deposited (mAh cm^2)	O (at. %)	Ti (at.%)	W (at. %)
TiO_2 (2 h)	2	0	72 ± 2	28 ± 2	0
WO_3/TiO_2 (1 h)	1	0.225	72 ± 1	25 ± 1	2.9 ± 0.4
WO_3/TiO_2 (2 h)	2	0.225	73 ± 1	15 ± 1	12 ± 1
WO_3/TiO_2 (5 h)	5	0.225	71 ± 1	23 ± 1	6.6 ± 0.1

different areas in the same sample in order to accurately represent the whole sample (A representative SEM-EDS image/spectrum can be seen in SI Figures S3 and S4). The main elements found in TiO_2 NTs were titanium and oxygen. However, for the WO_3/TiO_2 NTs, the tungsten peaks were predominant and very well-defined. The averaged atomic percentages for the main elements detected by EDS are summarized in Table 3. One interesting result is that the WO_3/TiO_2 materials with different Ti anodization time, but with the same WO_3 deposited charge obtained different morphology and W atomic percentages. When WO_3 is electrodeposited on flat surfaces (such as FTO glass), the resulting WO_3 film is a compact film with no defined structure. However, in our previous study, we showed that TiO_2 nanotubes act a skeleton to create defined nanostructures.[15] We showed that different nanostructures can be formed as a function of WO_3 electrodeposition time when TiO_2 NTs of the same length are used as substrate. With shorter electrodeposition time at higher current, as occurred for shorter tubes, the WO_3 particles were deposited around the TiO_2 nanotube walls, and with longer times at lower current, as occurred for longer tubes, WO_3 tubular nanostructures grew on top of the TiO_2 nanotubes.[15] In this work, the WO_3 deposited charge is the same and TiO_2 NTs of different lengths were used as substrate.

Figure 4 shows that WO_3 nanostructures obtained using TiO_2 NT with shorter anodization time (shorter nanotubes) look more compact and agglomerated than those using TiO_2 NT with longer anodization time (longer nanotubes) which looks

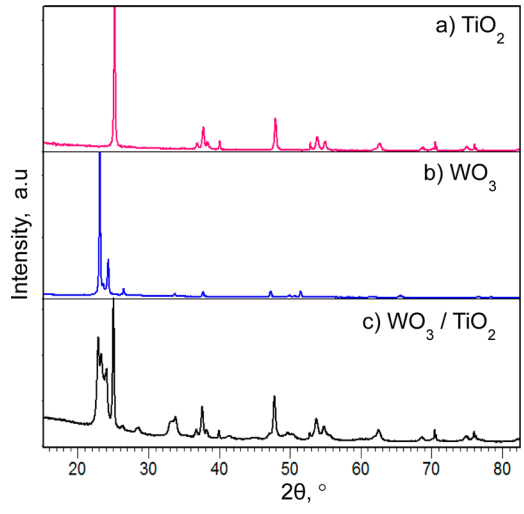

Figure 4. XRD of (a) TiO_2, (b) WO_3, and (c) WO_3/TiO_2 NT.

DOI: 10.1021/am5050696
ACS Appl. Mater. Interfaces 2015, 7, 2202–2213

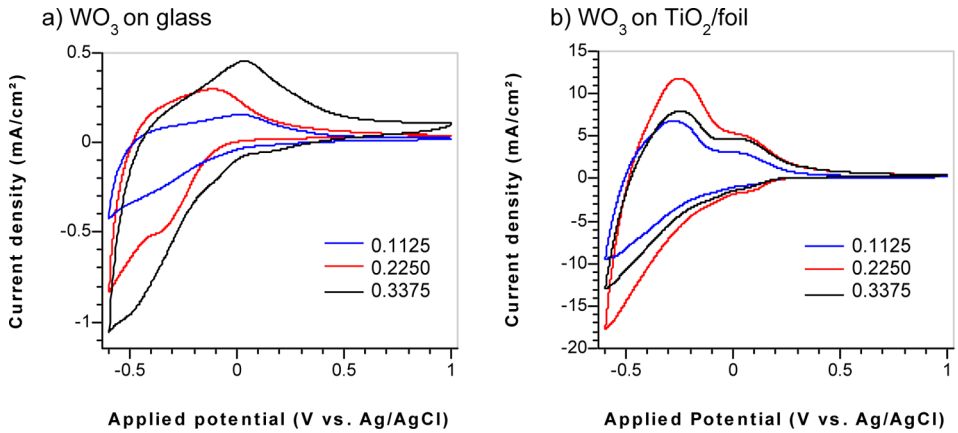

Figure 5. CV of (a) WO_3 electrodeposited on FTO glass and (b) on TiO_2 nanotubes (on foil) at different deposited charge densities of (0.3375, 0.225, and 0.1125 mA h cm^{-2}). All samples were tested in 0.1 M $HClO_4$ electrolyte solution at a scan rate of 40 mV s^{-1}.

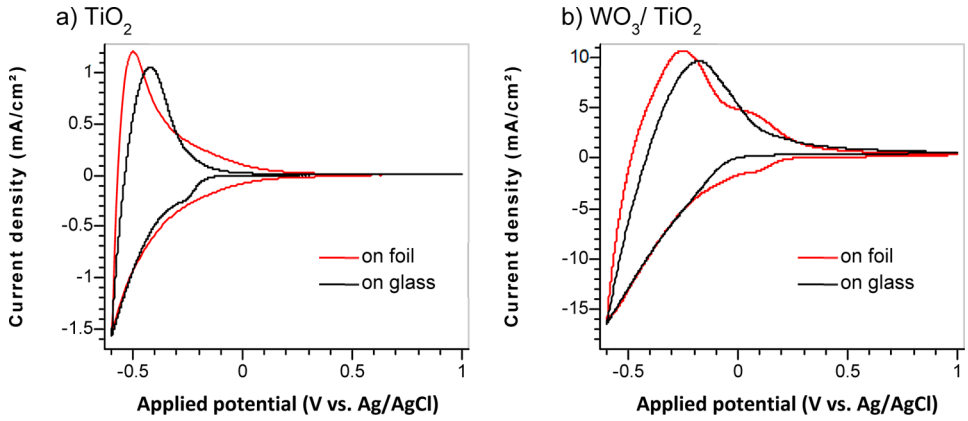

Figure 6. CV of (a) TiO_2 NT and (b) WO_3/TiO_2 NT before and after been transferred to glass. (a,b) the TiO_2 anodization time was 5 h and (b) WO_3 deposition charge was 0.225 mA·h/cm^2. P25 nanoparticles were used as adhesion layer. All samples were tested in 0.1 M $HClO_4$ electrolyte solution at a scan rate of 40 mV s^{-1}.

more like thinner nanostructures. EDS results indicate that W at % for WO_3/TiO_2 (1h), (2 h), and (5 h) was 2.9, 12 and 6.6%, respectively. For WO_3/TiO_2 (2 h), we believe that the W signal is higher and Ti signal is lower because the WO_3 film is denser, covering more of the TiO_2. We interpret these results as follows: with too short TiO_2 nanotubes, WO_3 particles deposit mainly on the upper surfaces of the nanotubes creating a dense layer, and with longer nanotubes, some WO_3 particles can grow to form their own nanostructured layer on top of the NT. This could explain why WO_3/TiO_2 (5 h) obtained a larger thickness than the bare TiO_2 (5 h). Due to the finite resistivity of TiO_2 tubes, the potential at the nanotube/electrolyte interface could be different with different nanotube length, and growth rates are clearly different for different tube lengths for a given applied potential. These differences in conditions could promote the creation of different structures.

3.2.2. Crystal Structure and Grain Size. Figure 4 shows the X-ray diffraction (XRD) patterns of TiO_2, WO_3 and WO_3/TiO_2 composite films, all of which had been annealed in air for 2 h at 450−500 °C. TiO_2 NTs show the distinct peaks for the anatase phase. No other XRD peaks except for substrate (FTO or Ti foil) peaks were detected, indicating a single crystalline compound. XRD patterns of TiO_2 NT on Ti foil collected before the detachment/transfer to the glass show the same anatase phase, indicating that the crystal structure is not affected by the detachment/transfer process. The WO_3 film showed three distinct peaks in the range 23° < 2θ < 25°. These three peaks can be observed in the WO_3 electrodeposited on FTO glass as well as on Ti foil. WO_3, despite its simple stoichiometry, can be found in large variety of crystal structures (e.g., monoclinic, orthorhombic, and triclinic). Comparing the XRD patterns with the JCPD reference files, the diffraction peaks resemble those of a monoclinic structure (JCPD # 43-1035), the most stable phase at room temperature. For the composite materials, the predominant sharp (2θ = 25°) can be assigned to TiO_2 anatase phase and the broad peaks (23° < 2θ < 25°) to the three WO_3 monoclinic peaks. No additional peaks were detected, indicating the absence of Ti−W alloys. There is negligible broadening of the TiO_2 peak. The refined crystallite size values are >100 nm, indicating there is essentially no peak broadening due to small grains in the material. Powder XRD patterns indicate significant peak broadening for the WO_3 phase, especially for the WO_3/TiO_2 nanocomposite. The average crystallite size of the WO_3 material electrodeposited on FTO is 76 nm, while the corresponding value for WO_3 grown on TiO_2 nanotubes is only 12 nm. The microstrain values are very small and do not seem to contribute significantly to the peak broadening.

3.3. Electrochromic Performance. *3.3.1. Current Density of WO_3/TiO_2 Materials.* Electrochromic materials change their color when an electrical voltage is applied. It is well-known that the insertion−extraction cycle of protons and electrons

DOI: 10.1021/am5050696
ACS Appl. Mater. Interfaces 2015, 7, 2202−2213

accounts for the coloring–bleaching reactions:[7,11] $WO_{3\ (bleached)} + xH^+ + xe^- \leftrightarrow H_xWO_{3\ (colored)}$ and $TO_{2\ (bleached)} + xH^+ + xe^- \leftrightarrow H_xTiO_{2\ (colored)}$. When a proton is inserted in the metal oxide lattice (TiO_2 or WO_3), the metal is reduced (from Ti^{4+} to Ti^{3+} for TiO_2 and W^{6+} to W^{5+} for WO_3) and the color changes from bleached to colored. In a CV, a cathodic peak indicates the potential range in which the proton inserts into the lattice, whereas the anodic peak is the potential range in which the colored material is oxidized to the original metal oxide.[7]

TiO_2 NTs with different lengths showed similar CVs, indicating that the nanotube length does not significantly affect the superficial current density of TiO_2 (SI Figure S5). This may be because only the outer surface of the tubes contributes to the current. A clear anodic peak can be seen around −0.5 V vs Ag/AgCl, and cathodic current is observed at more negative potentials.[11] To study how the WO_3 concentration affects the electrochromic performance, different concentrations were electrodeposited on FTO glass (without TiO_2 NT) and analyzed by CV. The anodic peak can be seen around 0.02 V and cathodic peak around −0.35 V vs Ag/AgCl for WO_3 materials. Figure 5(a) indicates that the current density increases with increasing WO_3 concentration, with about a 10% increase in maximum current density when the WO_3 deposited charge density increases from 0.225 to 0.3375 mA h cm^{-2}. The CV maximum current density vs deposited charge density slope is less than 1, suggesting either a deposition efficiency that decreases with thickness, or that deeper regions in the deposited film contribute less current to the CV. The CV for the composite materials on Ti foil (Figure 5b) shows two well-defined anodic peaks. On the basis of the CVs for the single material (Figure 5a and Figure 6a), we assigned the anodic peak at more negative potential to TiO_2 and the other one to WO_3. With higher WO_3 deposited charge, the TiO_2 peak decreased, suggesting that the WO_3 is covering more of the surface. The middle WO_3 concentration (0.225 mA h cm^{-2}) showed the higher charge density. This result agrees with our previous, work where WO_3/TiO_2 samples with moderate electrodeposition time produce the most active photoanode.[15] This result suggests that it is an optimal WO_3/TiO_2 ratio depending on which application these composite materials will be used for. As shown in Figure 5(b), when WO_3 is electrodeposited on TiO_2 NT membranes on Ti, the charge capacity is more than 20 times higher than the electrodeposited WO_3 on FTO (Figure 6 (a)). This result indicates that the underlying TiO_2 NTs and the WO_3/TiO_2 interface are sufficiently conductive to allow electrochemical reaction of the WO_3 external layer. Also this result shows significant enhancement due to the composite nanostructure.

WO_3/TiO_2 NTs with different WO_3 charges (0.2250 and 0.3375 mA·h/cm^2) and different anodization times (1, 2, and 5 h) were detached from the Ti foil and transferred to FTO glass. WO_3/TiO_2 NT membranes with different nanotubes lengths (different anodization times) showed similar CV. This result is in good agreement with the conclusion that only the outer surface of the tubes contributes to the current density. Figure 6 show a representative CV for TiO_2 NT and WO_3/TiO_2 NT before and after been transferred to FTO glass. The membranes on FTO have slightly lower current densities and similar reversibility to those of on Ti foil. These results suggest that the detachment/transfer techniques successfully retain the good charge transport capabilities with no significant negative effects on either ion storage capacity or redox reversibility. Figure 6a shows that the TiO_2 anodic peak shifted to more positive potential after it was transferred to glass. A small cathodic peak around −0.25 V vs Ag/AgCl can sometimes been seen for TiO_2 on glass, which we believe results from materials in the adhesion layer. Figure 7b shows that WO_3 and TiO_2

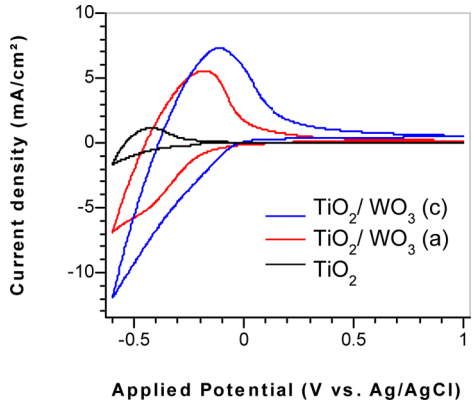

Figure 7. CV of the same sample at different sythetic stages (TiO_2 NT, amorphous (a) WO_3/TiO_2 and (c) crystalline WO_3/TiO_2) between 1 V and −0.6 V in 0.1 M $HClO_4$ electrolyte solution at a scan rate of 40 mV s^{-1}. TiO_2 NT anodization time was 5 h and WO_3 deposition charge was 0.225 mA/cm^2.

anodic peaks are not as well-defined as those for the same material on Ti foil. The thick P25 nanoparticle layer used as the adhesion layer could be affecting the electron transfer to the back of the electrode, causing the changing of the peak positions.

In summary, as shown in Figure 5 and Figure 6, WO_3/TiO_2 NT composite materials have ion storage capacities significantly higher than the single materials: approximately 10 times higher than TiO_2 nanotubes and 20 times higher than electrodeposited WO_3. This result indicates that combining these two materials not just adds to the current densities, but also significantly enhances the ion storage capacity due to the composite nanostructure. We believe that this is the highest reported current density to date for TiO_2, WO_3 and TiO_2–WO_3 composite electrochromic materials. Many other studies report the electrochromic enhancement of composite materials. Benoit et al. reported the "decoration" of TiO_2 nanotubes with WO_3 nanocrystals by the hydrolysis of WCl_6.[11] EC activity was measured in situ while the film was on the Ti substrate, and the TiO_2 NT with WO_3 on the surface had increased current densities, more distinct onset potentials, higher contrast, and higher ion intercalation capacity compared to pure TiO_2 NT.[11] The TiO_2 NT-WO_3 current density of the anodic peak increased by about 1 mA cm^{-2} compared to pure TiO_2 NTs, reaching values up to 1.25 mA/cm^2 at a scan rate of 50 mV/s in 0.1 M $HClO_4$ electrolyte. Our best material under similar experimental conditions reached a current density of 10 mA/cm^2. Nah et al. showed that composite TiO_2–WO_3 NTs can be fabricated by anodization of a TiW alloy. Their material, tested in situ on the TiW alloy substrate, has an ion storage capacity of 16.9 mC cm^{-2} for the anodic.[13] Our materials reached ion storage capacities higher than 65 mC cm^{-2} Recently, Cai et.al. reported the preparation of TiO_2@WO_3 core/shell nanorod arrays on FTO with enhanced electrochromic properties. The improvement was mainly attributed to the core/shell structure and the porous space among the nanorod array, which makes the ion diffusion become easier and it also gives larger surface area for charge-transfer reactions.[14] Using a scan rate of 20 mV/

DOI: 10.1021/am5050696
ACS Appl. Mater. Interfaces 2015, 7, 2202–2213

s in 0.5 M H_2SO_4 solution, their CV measurements showed that pure WO_3 on FTO has current densities around 0.25 mA/cm^2, which is in the same range of our results for pure WO_3 on the same substrate. However, the pure TiO_2 nanotubes and TiO_2@WO_3 materials showed significantly lower current densities than ours: less than 0.2 mA/cm^2 for pure TiO_2 and less than 1.0 mA/cm^2 for their best TiO_2@WO_3 materials. The TiO_2 nanorods reported by Cai et.al. have length up to 700 nm. Our TiO_2 nanotubes have lengths of several microns. The length of the TiO_2 nanotructures could be the reason why our materials show significantly higher current densities.

3.3.2. Amorphous vs Crystalline WO_3 on TiO_2 NT. Figure 7 shows the CV of the same sample on FTO glass in three different stages: TiO_2 NTs (before WO_3 electrodeposition), amorphous ("a") WO_3 /TiO_2 NTs (after WO_3 electrodeposition and before annealing), and crystalline ("c") WO_3 /TiO_2 NTs (after WO_3 electrodeposition and after annealing). Bare TiO_2 NTs showed the lowest peak current density, while crystalline WO_3 /TiO_2 NTs showed higher current density than amorphous WO_3/TiO_2 NTs.The peak current is reached when the film approaches its charge capacity, and it becomes difficult for charge to move deeper into the film. The slope of the forward scan where it crosses zero is steeper when the film is more conductive to the ions moving into it. The position of the peak will shift to later times and higher voltages if the charge capacity is greater, and the conductivity is the same. The height of the peak will also be greater. For a given charge capacity, the peak will be higher and earlier (occurring at lower voltage) if the conductivity is higher. The films in Figure 7 appear to have large increases in capacity and small increases in conductivity as further processing steps are applied.

However, Benoit et al. found that the charge density is slightly decreased due to the crystallinity of WO_3 nanoparticles.[11] The discrepancy could be due to the different synthetic approaches used that yield to different morphologies and grain sizes. The approach used in Benoit's work was the decoration of TiO_2 nanotube layers with WO_3 nanoparticles by the controlled hydrolysis of a WCl_6 precursor. Their final materials are open TiO_2 nanotubes covered with a hazy very thin WO_3 layer. Our approach creates completely different defined WO_3 nanostructures, including nanorods, nanowires, and coral-like structures and very small grain sizes (~12 nm). For our materials, the annealing step increases the ion uptake efficiency.

3.3.3. Cycling Stability. One important material property for any EC application is material stability over long periods of time. To the study the stability of these composite materials, CVs with 50 cycles were carried out. The charge capacities and peak positions are summarized in Table 4. As shown in Figure 8b, the charge capacity of WO_3 alone quickly decreases during the first 5 cycles. The anodic and cathodic peaks become less defined, and the ratio between the peaks changes from 0.37 to 0.24. When WO_3 is electrodeposited on FTO (WO_3/FTO), the film has poor stability. After few cycles using WO_3/FTO, blue particles of partially reduced WO_3 spontaneously detach from the FTO glass, and accumulate at the bottom of the electrochemical cell. The TiO_2 NT films appear visually identical after 50 cycles, with no evidence of detachment or degradation. However, as shown in Figure 8a and Table 4, the anodic peak position shifted to a positive potential and the ion capacity significantly decreased as a function of number of cycles. These results suggest a progressive irreversible intercalation in the TiO_2 lattice. In contrast, Figure 8c,d shows that the WO_3 film electrodeposited on TiO_2 NTs are very stable. Figure 8c shows minimal difference between the first and 50th cycle of WO_3/TiO_2 on Ti foil and Figure 8d shows that after the first cycle, the following CVs showed very small differences for WO_3/TiO_2 on glass. The anodic peaks position did not change after 50 cycles. Even after the composite were transferred to glass (Figure 8d), the composite materials showed a very good stability and robustness. With only 50 cycles we can determine that the single materials: TiO_2 NT and WO_3 are not stable and the WO_3/TiO_2 materials showed no signal of instability or degradation. XRD patterns show that the crystal structure of the WO_3/TiO_2 NT materials was the same before and after the proton intercalation After CVs using WO_3/TiO_2 NTs, the electrolyte solution and the bottom of the cell were always clear and there was no visible electrode degradation. Some of the WO_3/TiO_2 NTs have been used for multiple experiments and the performance has been very consistent.

Table 4. Charge Capacity and Peak Position after 50 Cycles[a]

sample label	cycles	Q_{anodic} (mC/cm^2)	anodic peak position (v)
WO_3	1	3.63	0.019
	50	0.814	0.193
TiO_2 NT	1	4.057	−0.511
	50	0.251	−0.194
WO_3/TiO_2 NT	1	68.49	−0.176
	50	73.24	−0.176

[a]Data calculated from CV in 0.1 M $HClO_4$ electrolyte solution at a scan rate of 40 mV s^{-1}. For all the samples, the substrate was FTO glass, TiO_2 NT anodization time was 5 h and WO_3 deposition charge was 0.225 mA/cm^2.

3.3.4. Switching Time. "Switching time" is the amount of time required to pass most of the charge when a voltage change is applied. Double potential step chronoamperometry (DPSC) was used to compare the switching times of different TiO_2 NT and WO_3/TiO_2 NT membranes on FTO glass. The films were cycled, alternating the potential from −1 to 1 V for 5 s intervals. The cathodic current densities correspond to the film darkening as protons and charge-balancing electrons move into the film. The anodic current densities correspond to the film bleaching. As shown in Figure 9, the composite WO_3/TiO_2 NTs showed the largest charge density compared with pure WO_3 and TiO_2 NTs, maintaining a relatively fast switching time (approximately 1 s to reach steady-state). Figure 9 (down) shows that WO_3 on glass and TiO_2 on Ti foil have faster responses (in the milliseconds range) than TiO_2 on FTO using P25 as adhesion layer (in the second range). This observation suggests that P25 nanoparticle layer could be increasing the switching time of WO_3/TiO_2 on glass. Figure 2 shows the adhesion layer could be thicker than the NT layer. It may be that thinner layers can still provide adequate adhesion while decreasing the switching time. For smart window applications, switching times on the order of seconds are adequate. However, for other applications (such as displays), switching times on the order of milliseconds are needed. For the potential use of these materials for displays application, the use of thinner P25 adhesion layers or new adhesion techniques are needed.

3.3.5. Electrochromic Contrast. The change in redox state can be correlated quantitatively with changes in optical properties. The samples used for the diffuse reflectance experiments were FTO glass with WO_3 electrodeposited on it, and the remainder of the membranes is composite materials

DOI: 10.1021/am5050696
ACS Appl. Mater. Interfaces 2015, 7, 2202−2213

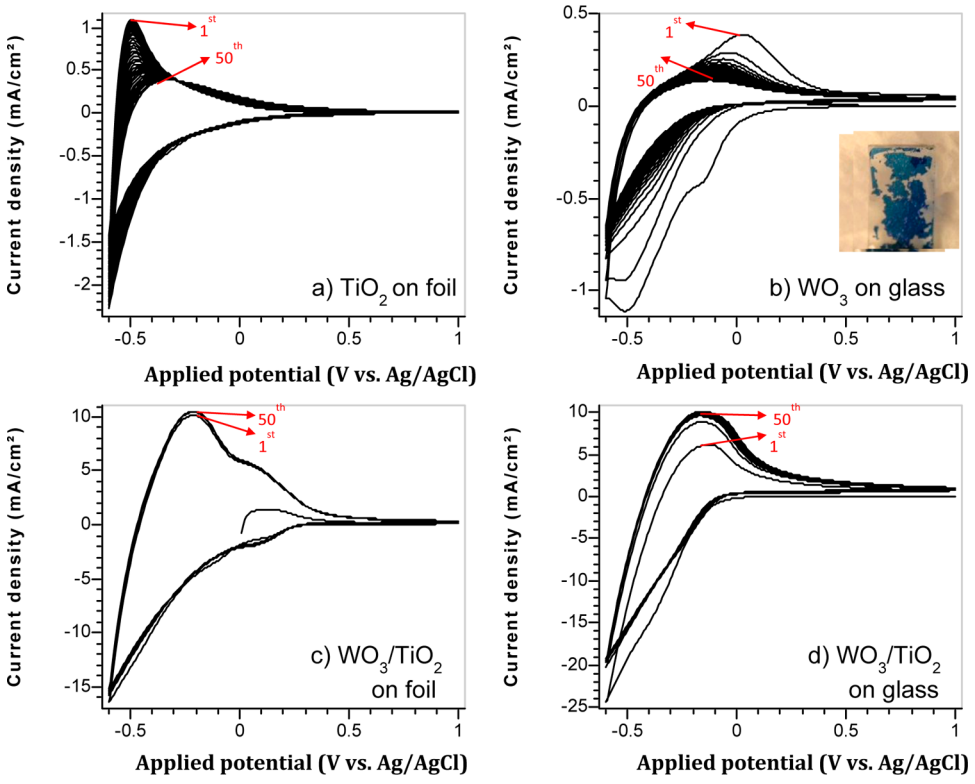

Figure 8. Fifty-cycle CV of (a) TiO_2 NT (5 h) on foil, (b) WO_3 on glass and WO_3/TiO_2 NT (5 h) (c) on foil and (d) on FTO glass in 0.1 M $HClO_4$ electrolyte solution at a scan rate of 40 mV s^{-1}. A photograph of the WO_3 on glass after 5 cycles was included.

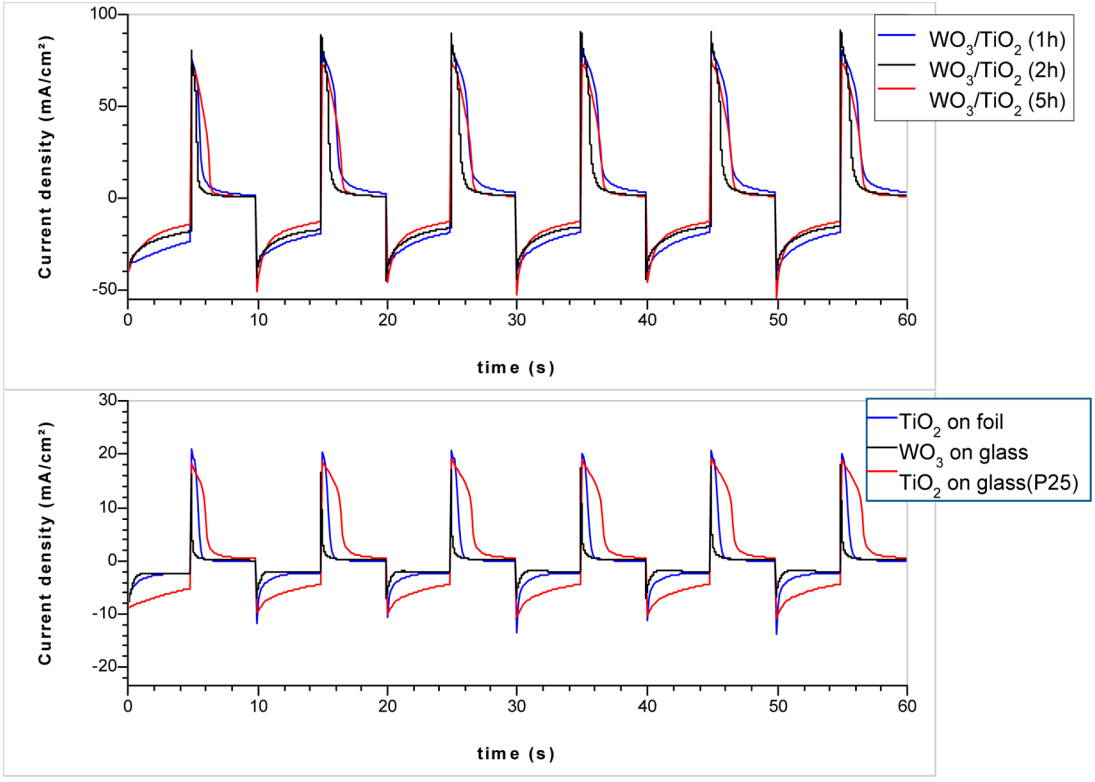

Figure 9. Alternating cycles from −1 to 1 V for 5 s intervals in 0.1 M $HClO_4$ electrolyte. All the electrodes are using P25 as adhesion layer to the FTO, except "TiO_2 on Ti foil".

of TiO_2 NTs attached with P25 paste onto FTO glass and WO_3 electrodeposited on the surface. For each of the samples in Figure 10, a photograph was taken and the diffuse reflectance spectrum was collected before the electrochromic testing in order to demonstrate the initial (bleached) state of the sample. Therefore, each sample was scanned from 1 V to −0.6 V at 40

DOI: 10.1021/am5050696
ACS Appl. Mater. Interfaces 2015, 7, 2202−2213

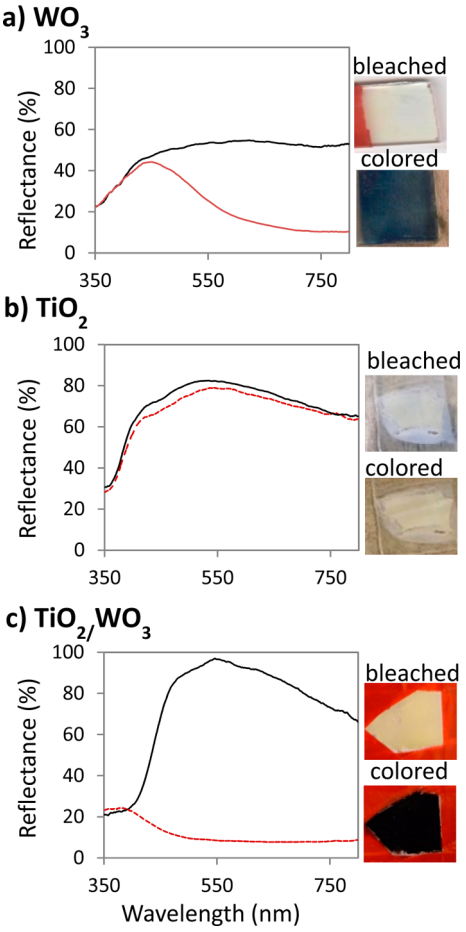

Figure 10. Total reflectance and photographs of (a) TiO_2 NT (5 h), (b) WO_3 on FTO glass with a concentration of 0.225 mA h cm^{-2} and (c) WO_3/TiO_2 NT (2 h) membrane with WO_3 concentration of 0.225 mA h cm^{-2} before and after a coloration cycle.

mV s^{-1} in 0.1 M $HClO_4$ electrolyte solution. Another photograph was taken at colored state, and the sample was placed inside the spectrometer as quickly as possible (around 5 min). Diffuse reflectance plots were shifted to match the initial diffuse reflectance of the material in the ultraviolet region to account any change due to sample loading or drying. In Figure 10, the reflectance spectra were plotted versus wavelength and photographs of the initial and final coloration states are included. In Table 5, the reflectance difference at 600 nm,

Table 5. Reflectance Difference (ΔR) at 600 nm and Time to Reach ΔR < 25% and ΔR < 0.1%

sample	ΔR (%)	time (h) ΔR < 25%	time (h) ΔR < 0.1%
TiO_2	3		1
WO_3	37	0.37	3
WO_3/TiO_2 (1 h)	49	0.57	6
WO_3/TiO_2 (2 h)	82	0.70	44
WO_3/TiO_2 (5 h)	70	0.73	44

which is the difference between the reflectance at the bleached state and at colored state (immediately after the coloration cycle) and time to reached negligible reflectance difference were summarized.

Bare WO_3 film (Figure 10a) has a high reflectance difference only at longer wavelength. The reflectance spectra show a gradual decrease in reflectance from 450 nm to a minimum at approximately 750 nm (ΔR < 37% at 600 nm). After the proton intercalation, the film changes from transparent to blue. As shown in Figure 10b, the reflectance difference of the reduced vs oxidized TiO_2 NTs is almost negligible (ΔR < 3% at 600 nm) and no significant visual color change can be discerned from the photographs. Figure 10c shows the electrochromic contrast of composite WO_3/TiO_2 NTs. The combination of these two materials has a big impact in EC in terms of the wavelength range. Compared to WO_3 on FTO glass, at colored state, the reflectance spectra show a flat minimal response throughout the entire visible range (400−800 nm). The postcoloration cycle photographs show that the material changed to a very dark color. As shown Table 5, WO_3/TiO_2 materials prepared with nanotubes with anodization times have a different electrochromic contrast. The ΔR at 600 nm for WO_3/TiO_2 samples with nanotubes of ∼6 μm (1 h), ∼12 μm (2 h), and ∼22 μm (5 h) was 49, 82, and 70%, respectively. According Table 3, the WO_3/TiO_2 (2 h) has the higher superficial W atomic % and obtained the higher electrochromic contrast. The length of the nanotubes, but also the concentration of WO_3 on the surface plays important roles in the electrochromic performance.

The reflectance difference is an indirect way to evaluate the relative electrochromic contrast among these materials. Benoit et al. also use reflectance difference to evaluate the electrochromic performance of TiO_2 nanotubes decorated with WO_3.[11] At 600 nm, the authors reported a ΔR (%) of 3% for neat TiO_2 nanotubes, which is in very good agreement with our results. For TiO_2 decorated with WO_3, they reported 45% for the as-formed and 21% for the annealed structure. Our materials showed significant higher ΔR (%). Absolute coloration efficiency could not be directly quantified for these semitransparent materials due to difficulty of direct transparency measurements because of the light scattering and haziness. For the majority of the electrochromic applications (expect for reflectance devices), high transparency at the bleached state is needed. The transparency of our materials could be increased if the thickness of adhesion layer (which is white and opaque by itself) and length of the nanotubes are decreased. As previously mentioned, transferring thinner membranes is challenging. It has been reported by Wang et al. that a through-hole TiO_2 nanotube array of 18 μm is transparent.[21] Opening the bottom of the nanotubes could increase the transparency, although it is still unknown how tis could affect the electron transfer to the substrate because these though-hole arrays have not been tested for electrochromic applications.

For some EC applications, such as smart windows, materials with a long memory time at open circuit are desirable because they can retain color for long periods without the need to reapply voltage. The reflectance difference was collected as a function of time for each sample (SI Figure S6). Table 5 also summarizes time elapsed from the colored state to back to the initial state at open circuit (ΔR < 0.1%). For all the materials, a significant color change (ΔR < 25%) occurred in the first hour. WO_3 followed by WO_3/TiO_2 NTs (1 h), WO_3/TiO_2 NTs (2 h) and finally WO_3/TiO_2 NTs (5 h) changes color the fastest directly after anodic bias. After 6 h the WO_3/TiO_2 NT (1 h) material and the WO_3 on FTO glass have very small values of reflectance difference. At 44 h, neither the WO_3/TiO_2 NTs (2 h), nor the WO_3/TiO_2 NTs (5 h), have completely reversed back to their initial states. This result indicates that the NTs

DOI: 10.1021/am5050696
ACS Appl. Mater. Interfaces 2015, 7, 2202−2213

increase the materials' abilities to retain charge relative to the nanoparticulate WO_3. These measurements are a way to compare the ability of our materials to retain color. These are not absolute memory time measurements because the electrodes were outside of the electrolyte and exposed to air. Real devices are sealed and protected from the ambient, which result in long memory times of weeks or months.

4. CONCLUSIONS

In this work, we showed that TiO_2 nanotubes can be used for the development of composite TiO_2/WO_3 materials with unique organized nanostructures and enhanced electrochromic activity. The TiO_2 NT can be detached and transferred to glass without losing its good electrical conductivity. The membranes on the glass were used as a substrate for in situ WO_3 electrodeposition. The composite WO_3/TiO_2 nanostructures showed 20 times higher ion storage capacity than neat WO_3 and 10 times higher than neat TiO_2 NT. Also, the composite materials showed higher electrochromic contrast compared with the pure WO_3 and TiO_2. In addition, the composite materials showed excellent cycling stability, a switching time in the second range and longer "memory time" under open-atmosphere conditions. The synthetic approach described in this work may prove useful for EC devices because it produces materials that perform well. Utility for smart window applications is limited by the translucent nature of the film. Further optimization of layer thickness, especially the adhesion layer, may lead to improved transparency. Such improved TiO_2 NT-on-glass electrodes may also find uses in other applications, such as dye-sensitized solar cells other cases where the photooxidative properties of TiO_2 are of value.

■ ASSOCIATED CONTENT

Supporting Information

CV of TiO_2 NT membranes on glass transferred with different techniques, SEM cross sectional images of TiO_2 NT membranes on P25 layer/glass, SEM plain-view images of TiO_2 NT and WO_3/TiO_2 NT membrane on glass and EDS spectra, and CV of TiO_2 NT with different anodization times and reflectance difference vs time. This material is available free of charge via the Internet at http://pubs.acs.org/.

■ AUTHOR INFORMATION

Corresponding Author

*E-mail: krreyes@sandia.gov.

Notes

The authors declare no competing financial interest.

■ ACKNOWLEDGMENTS

The authors want to thanks Nancy Yang, Jeffery M. Chames and Ryan Nishimoto for the SEM and EDS data collection. This work was supported by the Laboratory-Directed Research and Development program at Sandia National Laboratories, a multiprogram laboratory managed and operated by Sandia Corporation, a wholly owned subsidiary of Lockheed Martin Corporation, for the U.S. Department of Energy's National Nuclear Security Administration under contract DE-AC04-94AL85000.

■ REFERENCES

(1) Deb, S. K. Opportunities and Challenges in Science and Technology of WO_3 for Electrochromic and Related Application. *Sol. Energy Mater. Sol. Cells* **2008**, *92*, 245−258.
(2) Roy, P.; Berger, S.; Schmuki, P. TiO_2 Nanotubes: Synthesis and Applications. *Angew. Chem., Int. Ed.* **2011**, *50*, 2904−2939.
(3) Mortimer, R. J. Electrochromic Materials. *Annu. Rev. Mater. Res.* **2011**, *41*, 241−268.
(4) Monk, P. M. S.; Mortimer, R. J.; Rosseinsky, D. R. *Electrochromism: Fundamentals and Applications*; Wiley-VCH Verlag GmbH: Weinheim, 1995; Chapter 1, pp 5−15.
(5) Yu, Z.; Jia, X.; Du, J.; Zhang, J. Electrochromic WO_3 Films Prepared by a New Electrodeposition Method. *Sol. Energy Mater. Sol. Cells* **2000**, *64*, 55−63.
(6) de Tacconi, N. R.; Chenthamarakshan, R. C.; Rajeshwar, K. Electrochromic Behavior of WO_3, TiO_2, and Composite WO_3−TiO_2 Films Prepared by Pulsed Electrodeposition. *Proc.−Electrochem. Soc.* **2003**, *17*, 28−39.
(7) Wang, K.; Zeng, P.; Zhai, J.; Liu, Q. Electrochromic Films with a Stacked Structure of WO_3 Nanosheets. *Electrochem. Commun.* **2013**, *26*, 5−9.
(8) Zhang, J.; Tu, J. P.; Cai, G. C.; Du, G. H.; Wang, X. L.; Liu, P. C. Enhanced Electrochromic Performance of Highly Ordered, Macroporous WO_3 Arrays Electrodeposited Using Polystyrene Colloidal Crystals as Tempelate. *Electrochim. Acta* **2013**, *99*, 1−8.
(9) Nah, Y.-C.; Ghicov, A.; Kim, D.; Schmuki, P. Enhanced Electrochromic Properties of Self-organized Nanoporous WO_3. *Electrochem. Commun.* **2008**, *10*, 1777−1780.
(10) Zhang, J.; Tu, J.; Du, G.; Dong, Z.; Wu, Y.; Chang, L.; Xie, D.; Cai, G.; Wang, X. Ultra-thin WO_3 Nanorod Embedded Polyaniline Composite Thin Film: Synthesis and Electrochromic Characteristics. *Sol. Energy Mater. Sol. Cells* **2013**, *114*, 31−37.
(11) Benoit, A.; Paramasivam, I.; Nah, Y. C.; Roy, P.; Schmuki, P. Decoration of TiO_2 Nanotube Layers with WO_3 Nanocrystals for High-Electrochromic Activity. *Electrochem. Commun.* **2009**, *11*, 728−732.
(12) Lai, C. W.; Sreekantan, S.; San, E. P. Effect of Radio Frequency Sputtering Power on W−TiO_2 Nanotubes to Improve Photoelectrochemical Performance. *J. Mater. Res.* **2012**, *27*, 1695−1704.
(13) Nah, Y.-C.; Ghicov, A.; Kim, D.; Berger, S.; Schmuki, P. TiO_2−WO_3 Composite Nanotubes by Alloy Anodization: Growth and Enhanced Electrochromic Properties. *J. Am. Chem. Soc.* **2008**, *130*, 16154−16155.
(14) Cai, G. F.; Zhou, D.; Xiong, Q. Q.; Zhang, J. H.; Wang, X. L.; Gu, C. D.; Tu, J. P. Efficient Electrochromic Materials Based on TiO_2@WO_3 Core/Shell Nanorodarrays. *Sol. Energy Mater. Sol. Cells* **2013**, *117*, 231−238.
(15) Reyes-Gil, K. R.; Robinson, D. B. WO_3-Enhanced TiO_2 Nanotube Photoanodes for Solar Water Splitting with Simultaneous Wastewater Treatment. *ACS Appl. Mater. Interfaces* **2013**, *5*, 12400−12410.
(16) Ito, S.; Chen, P.; Comte, P.; Nazeeruddin, M. K.; Liska, P.; Péchy, P.; Grätzel, M. Fabrication of screen-printing pastes from TiO_2 powders for dye-sensitised solar cells. *Prog. Photovoltaics* **2007**, *15*, 603−612.
(17) Li, L.; Chen, Y.; Wu, H.; Wang, N. S.; Diau, E. W. Detachment and Transfer of Ordered TiO_2 Nanotube Arrays for Front-Illuminated Dye-Sensitized Solar Cells. *Energy Environ. Sci.* **2011**, *4*, 3420−3425.
(18) Albu, S. P.; Ghicov, A.; Schmuki, P. Lift Off Strategies for Self-Organized TiO_2 Nanotube Layers. *ECS Trans* **2009**, *16*, 195−202.
(19) Albu, S. P.; Ghicov, A.; Macak, J. M.; Hahn, R.; Schmuki, P. Self-Organized, Free-Standing TiO_2 Nanotube Membrane for Flow-through Photocatalytic Applications. *Nano Lett.* **2007**, *7*, 1286−1289.
(20) Liu, G.; Hoivik, N.; Wang, K.; Jakobsen, H. A Voltage-Dependent Investigation on Detachment Process for Free-Standing Crystalline TiO_2 Nanotube Membranes. *J. Mater. Sci.* **2011**, *46*, 7931−7935.
(21) Wang, D.; Liu, L. Continuous Fabrication of Free-Standing TiO_2 Nanotube Array Membranes with Controllable Morphology for

DOI: 10.1021/am5050696
ACS Appl. Mater. Interfaces 2015, 7, 2202−2213

Depositing Interdigitated Heterojunctions. *Chem. Mater.* **2010**, *22*, 6656−6664.
(22) Lei, B.; Liao, J.; Zhang, R.; Wang, J.; Su, C.; Kuang, D. Ordered Crystalline TiO_2 Nanotube Arrays on Transparent FTO Glass for Efficient Dye-Sensitized Solar Cells. *J. Phys. Chem. C* **2010**, *114*, 15228−15233.
(23) Park, J. H.; Lee, T.-W.; Kang, M. G. Growth, Detachment and Transfer of Highly-Ordered TiO_2 Nanotube Arrays: Use in Dye-Sensitized Solar Cells. *Chem. Commun.* **2008**, *25*, 2867−2869.
(24) Reyes, K. R.; Stephens, Z. D.; Robinson, D. B., Composite WO_3/TiO_2 Nanostructures for High Ecetrochromic Activity, Sandia National Laboratories, 2013, Report number: SAND2013-4494.

DOI: 10.1021/am5050696
ACS Appl. Mater. Interfaces 2015, 7, 2202−2213